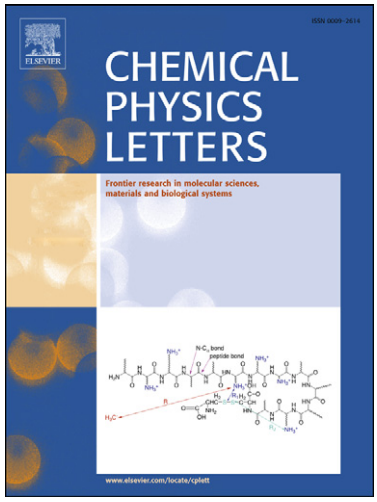

Evolution of magnetic nanophases of Ni embedded in Al_2O_3 (001) matrix by x-ray magnetic circular dichroism

P. Thakur, Ravi Kumar, J.C. Cezar, N.B. Brookes, Aditya Sharma, S.K. Arora, S. Gautam, Arvind Kumar, K.H. Chae, I.V. Shvets

PII: S0009-2614(10)01493-4
DOI: 10.1016/j.cplett.2010.11.027
Reference: CPLETT 28786

To appear in: *Chemical Physics Letters*

Received Date: 11 August 2010
Accepted Date: 10 November 2010

Please cite this article as: P. Thakur, R. Kumar, J.C. Cezar, N.B. Brookes, A. Sharma, S.K. Arora, S. Gautam, A. Kumar, K.H. Chae, I.V. Shvets, Evolution of magnetic nanophases of Ni embedded in Al_2O_3 (001) matrix by x-ray magnetic circular dichroism, *Chemical Physics Letters* (2010), doi: 10.1016/j.cplett.2010.11.027

Evolution of magnetic nanophases of Ni embedded in Al_2O_3 (001) matrix by x-ray magnetic circular dichroism

P. Thakur[a,*)], Ravi Kumar[b,)], J. C. Cezar[a], N. B. Brookes[a] Aditya Sharma[c], S. K. Arora[d], S. Gautam[e], Arvind Kumar[f], K. H. Chae[e], I. V. Shvets[d]**

[a]*European Synchrotron Radiation Facility, BP 220, F-38043 Grenoble Cedex, France*

[b]*Centre for Materials Science and Engineering, National Institute of Technology, Hamirpur 177005 (H.P), India*

[c]*Material Science Research Laboratory, Department of Physics, S. V. College, Aligarh 202001 (U.P) India*

[d]*CRANN, School of Physics, Trinity College Dublin, Dublin 2, Republic of Ireland*

[e]*Nano Analysis Center, Korea Institute of Science and Technology (KIST), Seoul 136-791, Republic of Korea*

[f]*Beant College of Engineering & Technology, Gurdaspur 143521, India*

We report on the element-specific magnetic characterization of Ni nanoparticles (NPs) embedded in Al_2O_3(001) matrix prepared by ion-implantation (Ni:5×10^{16}-2×10^{17} ions cm^{-2}) technique. The x-ray diffraction studies reveal the coexistence of fcc Ni NPs of average size ~8-19 nm along with the other NiO_x phases. X-ray magnetic circular dichroism (XMCD) experiments demonstrate the competing nature of magnetic interactions between the Ni NPs and NiO_x phases. The ferromagnetism at 10 K (for all the Ni implants) is related to the combined contribution of both phases, while the room temperature superparamagnetism at higher fluence is dominated by Ni NPs phase as confirmed by Ni $L_{3,2}$ XMCD measurements.

* Correspondence author. Electronic email: thakur@esrf.fr (P. Thakur).

** On extraordinary leave from Inter University Accelerator Center, New Delhi-110067.

A common characteristic of metal/metal oxide nanostructured magnetic materials [so-called magnetic nanoparticles (NPs)] is the coexistence of two or more phases, magnetically and/or structurally different, which are modulated on a length scale of the order of a nanometer. Interactions between different magnetic phases of NPs have attracted both fundamental and technological research interest, motivated by the challenge of discovering and understanding phenomena related to the finite-size effects, surface/interface effects, including symmetry breaking and lattice-host exchange interactions [1-3]. There has been a great deal of recent interest in the incorporation of metal or metal oxide NPs into dielectric and semiconductor matrices to form nanocomposites [4-12]. Metal NPs in dielectric matrix could have potential applications in nonlinear optics and high density magnetic storage devices or magnetic sensors [13,14]. Various synthesis routes of ferromagnetic NPs fabrication are being currently employed and continuously improved; the aim is to improve the control over the size distribution, surface morphology, and stability of nanostructures. Negative-ion implantation is one of the promising method to fabricate metal NPs, because of little surface charging, high-purity process and good controllability in fluence, spatial position and depth [15]. In spite of huge efforts in the fabrication and characterization techniques of metal NPs, there are many unanswered questions concerning the development of magnetic order on a microscopic scale. In this context, the spin-dependent coupling mechanisms and the presence of surrounding medium (electronic environment/charge transfer) play an important role in determining their magnetic properties.

In this letter, we present the x-ray absorption (XAS) and x-ray magnetic circular dichroism (XMCD) characterizations of Ni NPs embedded in the sapphire (Al_2O_3-001) matrix prepared by Ni ion beam implantation. We study the systematic evolutions of magnetic phases of Ni NPs as a function of different Ni fluences and their magnetic response in the presence of other NiO_x phases.

Implantation of 80 keV Ni^- ions (current density of 1.5 μA cm^{-2}) was performed in a Al_2O_3 matrix at room temperature (RT) in a vacuum chamber of 1.3×10^{-7} Torr using source of negative ions by Cesium sputtering at Inter University Accelerator Centre, New Delhi. The implantation fluence was varied in the range of 5×10^{16} to 2×10^{17} ions cm^{-2}. Then the implanted samples were post-annealed in air at 600^oC for 4 hours to recover from radiation/structural damage caused by ion-implantation. According to Monte-Carlo ion-range simulation code SRIM2006, the projected range and straggling of Ni ions of 80 keV are ~38 nm and ~11 nm, respectively, in Al_2O_3 matrix. The formation of the Ni nanostructures was observed initially by high-resolution x-ray diffraction (HRXRD) with λ = 1.5425 Å, at the bending magnet 10B XRS KIST-PAL beamline of the Pohang Accelerator Laboratory (PAL). Figure 1 shows the HRXRD patterns (in log scale) for all the implants (Ni: 5×10^{16} - 2×10^{17} ions cm^{-2}) along with the bare Al_2O_3 substrate. As evident, a characteristic peak at $2\theta = 44.5^0$ corresponding to the fcc phase of Ni(111) is clearly observed. In addition to the fcc Ni (111) phase, pattern also shows the presence of other Ni oxide phases (NiO_x) [16], which are at variance with Ni fluences (marked by symbol "*" in the Fig. 1). It is well known that the crystal structure of Ni and its NiO_x phases is same and only the lattice parameters are different, therefore, Ni/NiO_x Bragg`s reflections occur at different 2θ values. From the diffraction profile analysis of the Ni (111) peak, an average size of Ni nanostructures (Ni: 5×10^{16} - 2×10^{17} ions cm^{-2}) was calculated to be ~8-19 nm by using Scherrer relation ($D = 0.9\lambda/\beta \cos\theta$, where β is the full width at half maximum of 2θ in radians). We have also estimated the average size of the other NiO_x phases as to be ~4-5 nm for all the samples. It is interesting to observe that there is no major increase in its value with the increase in implantation dose.

To understand the bulk magnetic properties of Ni NPs, the isothermal magnetization hysteresis measurements were performed at different temperatures (10-300 K) using a

vibrating sample magnetometer (Quantum Design- Physical Property Measurements System, USA) with a sensitivity of 5×10^{-7} emu. Figure 2 shows the magnetization versus magnetic field (M-H) curve for all the implants at 10 K (top panel) and 300 K (bottom panel). The diamagnetic contribution from the Al_2O_3 was subtracted from the measured data by performing the magnetization of the un-implanted Al_2O_3 sample with similar dimensions at RT. The M-H data presented in the Fig.2 is normalized with respect to the higher implantation fluence (Ni:2×10^{17} ions cm^{-2}). As evident, samples exhibits a well defined magnetization hysteresis and show ferromagnetic behavior at 10 K and their magnetic response increases with the Ni fluences. However, the magnetic properties of the implants at RT is very intriguing, the lower fluence samples show a weak ferromagnetism with observable coercive force and magnetic remanence, while the higher fluence (Ni:2×10^{17} ions cm^{-2}) sample exhibits a superparamagnetic like behavior. It is recalled that the surface morphology and magnetic domain formation of all the implants was also investigated by atomic force microscopy (AFM)/ magnetic force microscopy (MFM) using Digital Nanoscope-III. As a representative, insets in the Fig. 2 display the AFM (bottom panel) and MFM (top panel) images taken at RT for the higher fluence (Ni:2×10^{17} ions cm^{-2}) sample. A surface roughness was estimated to be ~13 nm (through AFM), while MFM image (taken at the 30 nm lift height of the tip) shows the corresponding magnetic contrast of the implants. It is worth mentioning that before annealing no AFM/MFM structure was observed for any implantation dose. The observed MFM image can be characterized by darker regions adjacent to the brighter regions in the nanometer scale and the magnetic regions are seems to be distributed uniformly along the plane of the Al_2O_3 matrix. The average contrast between dark and bright areas is measured by means of section analysis [17]. From the analysis of the MFM data, we have calculated the corresponding root mean square (RMS) phase shift of the as-implanted/annealed samples. The value of phase shift is found to be increased systematically from ~1.01^o (as-implanted

samples) to ~1.75°-2.54° (Ni:5×10^{16} - 2×10^{17} ions cm^{-2}) for the annealed samples, which undoubtedly indicates the formation of magnetic nanostructure of the Ni implants at the surface of the Al_2O_3 matrix. Since all the samples exhibit fluence/temperature dependent magnetic properties, we have carried out the zero-field-cooling (ZFC) and field-cooling (FC) magnetization as a function of the temperature (5-300 K). Figure 3 shows the ZFC and FC curves of the Ni implants (Ni:5×10^{16} and 2×10^{17} ions cm^{-2}) recorded with an applied magnetic field of μ_oH = 10 mT. In these ZFC/FC curves, the temperature at the position with maximum magnetization is known as the blocking temperature (T_B), above which the sample loses all its hysteric response. As evident, the higher fluence sample shows a superparamagnetic behavior above T_B~180 K, while the low fluence samples are ferromagnetic at RT. This can be related to the competing nature of magnetic interactions between fcc Ni(111) NPs and NiO_x phases. We will show in the following that the fluence-dependent destabilization of magnetism in the Ni NPs, and the presence of other NiO_x phases are playing an important role in determining their magnetic properties.

In order to investigate the structural/chemical environment of Ni NPs and its subsequent influence on the magnetic behavior with increasing fluence, we have carried out XAS and XMCD measurements at the Ni $L_{3,2}$ edge. The XAS/XMCD experiments were performed at the ESRF`s ID08 beamline, which uses an APPLE II type undulator giving ~ 100 % linear/circular polarization. All scans were recorded simultaneously in both total electron yield (TEY) and total fluorescence yield (TFY) modes, ensuring both surface (TEY) and bulk (TFY) sensitivities. The spectra were normalized to incident photon flux and the base pressure of the experimental chamber was better than 3×10^{-10} Torr. The samples were aligned at an angle of 45° between the surface normal and the incident beam. Since Ni NPs are embedded in the insulating matrix (Al_2O_3), the surface charging effect of the samples was severe in the TEY mode. Moreover, to avoid contributions from the surface contaminations

(air exposure etc.), all the spectra presented here are in the TFY mode. It should be noted that the absence of any surface contribution to the TFY mode spectra was further confirmed by performing XAS/XMCD experiments of the in-situ sputtered samples with an Ar^+ ion beam (1 KeV, 3.5 μA, 30 min.). Figure 4 shows the circularly polarized XAS spectra (μ^+ and μ^-) in the photon energy region of the Ni $L_{3,2}$ absorption collected in TFY mode for the lower fluence (Ni:5×10^{16} ions cm^{-2}) sample. A similar XAS spectra were observed for the other implants (not shown here). The corresponding XMCD spectra for all the implants at 10 and 300 K, defined as μ^+-μ^-, as shown in the Fig. 4 are collected with an applied magnetic field of ±5 T generated by a split coil superconducting magnet. Here, $\mu^+(\mu^-)$ refers to the absorption coefficient for the photon helicity parallel (antiparallel) to the Ni 3d majority spin direction. As a result of spin-orbit coupling in the 2p state, the spectra display two prominent features in the energy range of 845-860 eV (marked by A-C) and 865-875 eV (marked by D, E), respectively, corresponding to the L_3 ($2p_{3/2}\rightarrow3d$) and L_2 ($2p_{1/2}\rightarrow3d$) absorptions. As a guide, the reference XAS (top panel) and XMCD (bottom panel) spectra of metallic Ni thin films collected under the same experimental conditions are also shown in the Fig. 4 for comparison. The XMCD spectrum of pure NiO phase collected at 10 K is also shown in the lower panel of the Fig.4. The observed XAS spectra of the implants (Ni: 5×10^{16} - 2×10^{17} ions cm^{-2}) are closely resemble to the ionic multiplet structure of Ni [18], however XMCD spectral features are different to that of either pure Ni metal or NiO_x [18]. An inspection of XMCD spectra at the Ni L_3 edge shows that the peak A is due to metallic phase of the Ni NPs, while peaks B and C corresponds to the NiO_x phases in the samples (similarly at the Ni L_2 edge, peak D is due to the Ni NPs and peak E corresponds to the NiO_x phases). It should be noted that all the XMCD spectra presented in the Fig. 4 are normalized with respect to the Ni L_3 edge jump (peak B). At 10 K, it is clear that the XMCD signal of the peak A (associated to the Ni NPs) increases systematically with the Ni ion fluences, while the magnetic signal of the peaks B

and C (associated to the other NiO_x phases) is almost constant. The magnetic behavior of these peaks is reversed at RT as compared to that of low temperature (XMCD signal due to the peak A is almost constant, while the magnetic signal of the peaks B and C decreases with the Ni ion fluences). These results suggest that the magnetic properties of the implants are strongly depending upon the Ni ion fluences and can be correlated to the fluence-dependent magnetic contributions of the Ni NPs and NiO_x phases towards the total magnetic moment of the system.

In order to see the systematic evolution of these magnetic nanophases as a function of Ni fluences, we have performed the XMCD measurements at different temperatures (10-300 K). Figure 5 shows the temperature dependence of XMCD data collected in TFY mode for all the implants, while inset in the Fig. 5 (bottom panel) displays the hysteresis curve of the peak A (associated to the Ni NPs phase) at 10 K for the higher fluence sample. A similar hysteresis curve was obtained at the peak B (associated to the other NiO_x phases), which demonstrate that the NiO_x phases at low temperature have ferromagnetic components in all the implants (data not shown here). From the Fig. 5, it is clearly seen that the magnetic contribution of NiO_x phases for the higher fluence (Ni: 2×10^{17} ions cm^{-2}) sample continuously decreases with temperature and then almost disappear at RT. At low fluences (Ni: 5×10^{16} and 7×10^{16} ions cm^{-2}), samples still show an observable magnetic contribution of the NiO_x phases at RT. Since the higher fluence sample shows a superparamagnetic behavior at RT with bulk magnetometry (see Fig. 2 & Fig. 3) having a blocking temperature of T_B~180 K, therefore, it is reasonable to consider that this superparamagnetism is dominated by the Ni NPs phase apart from small contributions from the other NiO_x phases that may not be accessible within the sensitivity (smaller than 0.1% of the 3d metal) of XAS/XMCD spectroscopy. In other words, the thickness (volume) of NiO_x at higher fluence is not enough to pin the moments of Ni NPs. As the remanence of the implants at RT decreases with increasing Ni fluence during

implantation (increasing fcc-Ni particle size), this destabilization of the magnetism in Ni NPs can be attributed to a fluence-dependent NiO_x blocking temperature, above which magnetization is unstable [19]. We believe that at low fluences the NiO_x phase is blocked and stabilizes the magnetic moment of adjacent Ni NPs, while at high fluence the NiO_x is above the blocking temperature. These results were further confirmed by performing RT XMCD hysteresis loops at the peak B indicating a loss of NiO_x blocking with increasing Ni fluence (data is not shown here due to poor signal to noise ratio in the TFY mode). Another possible scenario is that at higher fluence the amorphization of the surrounding Al_2O_3 matrix may reduce the effective anisotropy of the Ni NPs leading to a reduction of the blocking temperature. A similar amorphization effect at higher fluence has been predicted by Xiang et al. in this system [6]. However, we have used here different synthesis conditions like; (a) the use of negative Ni ions during implantation (it helps to avoid surface charging effect and good controllability in fluence) and (b) the post-annealing of the samples in air at 600^{o}C for 4 hours, which have indeed helped to recover from the radiation/structural damage caused by the ion implantation as such no amorphization effects can be seen from the HRXRD and AFM/MFM data. Thus the embedded Ni NPs exhibits a fluence-dependent transition from ferromagnetic to superparamagnetic state and the NiO_x phases are playing an important role in determining their magnetic properties. It is worth noting that the observed magnetic properties of Ni NPs and NiO_x can be attributed to the presence of either (i) individual Ni and NiO_x particles in the samples, or (ii) Ni-NiO_x particles in a core-shell morphology with the NiO_x acting as a passivating layer [20]. However, our magnetic and XMCD data do not support (i) due to the fluence/temperature dependent magnetic interactions between Ni NPs and NiO_x phases. Moreover, the hysteresis loops displayed in the Fig. 2, and in the inset of Fig. 4 show that these loops are symmetric about zero field (without any exchange bias) indicating the absence of Ni NPs with core-shell Ni-NiO_x morphology. These exchange bias effects were

checked in both the FC/ZFC magnetization conditions. However, core-shell morphology without any exchange bias in this system can not be completely ruled out. In our opinion, such peculiarities of magnetic phenomenon in this system demands further XMCD experiment on the similar systems, especially metal NPs embedded in dielectric/insulating oxide matrices, to model these complex magnetic interactions between Ni NPs and NiO_x phases.

In summary, the element-specific magnetic properties of the Ni NPs embedded in Al_2O_3 (001) matrix prepared by ion-implantation technique have been investigated by performing XAS/XMCD measurements at the Ni $L_{3,2}$ edge. It is observed that all the implants exhibits ferromagnetism at 10 K due to magnetic contribution of both the phases (Ni NPs and NiO_x), while the room temperature superparamagnetism at higher fluence is dominated by Ni NPs phase. This destabilization of the magnetism in Ni NPs is attributed to a fluence-dependent NiO_x blocking temperature. Our XMCD data provide a distinct "fingerprint" for the complex magnetic interactions between the nanophases of Ni NPs and NiO_x. From a methodological point of view, we illustrate how the XMCD may be used as a suitable tool to study the embedded metal NPs into dielectric/insulating matrices and to distinguish the magnetic contribution of different phases.

[1] H. Kachkachi, M. Dimian, Phys. Rev. B **66**, 174419 (2002).

[2] L. Berger, Y. Labaye, M. Tamine, J. M. D. Coey, Phys. Rev. B **77**, 104431 (2008).

[3] H. Brune, P. Gambardella, Surface Science **603**, 1812 (2009).

[4] H. Amekura, N. Umeda, Y. Takeda, J. Lu, N. Kishimoto, Appl. Phys. Lett. **85**, 1015 (2004).

[5] A. Meldrum, R. F. Jr. Haglund, L. A. Boatner, C. W. White, Adv. Mater. **13**, 1431 (2001).

[6] X. Xiang, X. T. Zu, S. Zhu, L. M. Wang, Appl. Phys. Lett. **84**, 52 (2004).

[7] S. Zhu, L. M. Wang, X. T. Zu, X. Xiang, Appl. Phys. Lett. **88**, 043107 (2006).

[8] S. Zhou, G. Talut, K. Potzger, A. Shalimov, J. Grenzer, W. Skorupa, M. Helm, J. Fassbender, E. Čižmár, S. A. Zvyagin, J. Wosnitza, J. Appl. Phys. **103**, 083907 (2008).

[9] S. K. Sharma, P. Kumar, Ravi Kumar, M. Knobel, P. Thakur, K. H. Chae, W. K. Choi, R. Kumar, D. Kanjilal, J. Phys.: Condens. Matter **20**, 285211(2008).

[10] H. Amekura, K. Kono, Y. Takeda, N. Kishimoto, Appl. Phys. Lett. **87**, 153105 (2005).

[11] L.G. Jacobsohn , J. D. Thompson, R.M. Dickerson, M. Nastasi, Nucl. Instr. and Meth. B **169**, 141 (2000).

[12] K. Rumpf, P. Granitzer, P. Pölt, S. Šimić, H. Krenn, Phys. Stat. Sol. **205**, 1354 (2008).

[13] R. Lopez, T.E. Haynes, L.A. Boatner, L.C. Feldman, R.F. Haglund, Opt. Lett. **27**, 1327 (2002).

[14] R.P. Cowburn, J. Magn. Magn. Mater. **242–245**, 505 (2002).

[15] J. Ishikawa, H. Tsuji, Y. Toyota, Y. Gotoh, K. Matsuda, M. Tanjyo, S. Sakaki, Nucl. Instrum. Methods Phys. Res. B **96**, 7 (1995).

[16] S. Han, H.-Y. Chen, C.-C. Chen , Ta-Nien Yuan, H. C. Shih, Materials Letters **61** 1105 (2007).

[17] Z.H. Wang, K. Chen, Y. Zhou, H.Z. Zeng, Ultramicroscopy **105**, 343 (2005).

[18] G. van der Laan, C. M. B. Henderson, R. A. D. Pattrick, S. S. Dhesi, P. F. Schofield, E. Dudzik, D. J. Vaughan, Phys. Rev. B **59**, 4314 (1999).

[19] K. Nielsch, R. B. Wehrspohn, J. Barthel, J. Kirschner, U. Gösele, S. F. Fisher, H. Kronmüller, Appl. Phys. Lett. **79**, 1360 (2001).

[20] A. Roy, V. Srinivas, S. Ram, J. A. De Toro, U. Mizutani, Phys. Rev. B **71**, 184443 (2005).

Figure Captions

FIG. 1. HRXRD pattern of all the implants (Ni: 5×10^{16} - 2×10^{17} ions cm^{-2}) in Al_2O_3 matrix. A characteristic peak at $2\theta = 44.5^0$ corresponding to the fcc phase of Ni(111) is clearly visible along with other NiO_x peaks marked with symbol "*".

FIG. 2. Hysteresis loop (M-H curve) of all the implants measured at 10 and 300 K. Insets provide the AFM (bottom panel) and MFM (top panel) images for the higher fluence (Ni: 2×10^{17} ions cm^{-2}) sample.

FIG. 3. ZFC and FC magnetizations as a function of temperature for the lower fluence (Ni: 5×10^{16} ions cm^{-2}) and higher fluence (Ni: 2×10^{17} ions cm^{-2}) samples. Curves were recorded in the ZFC and FC processes at $\mu_oH = 10$ mT.

FIG. 4. Ni $L_{3,2}$ edge XAS (top panel)/XMCD (middle and bottom panel) spectra of all the implants (Ni: 5×10^{16} - 2×10^{17} ions cm^{-2}) measured at 10 and 300 K. Reference spectra of pure Ni metal and Ni oxide are also shown for comparison.

FIG. 5. Temperature dependence of Ni $L_{3,2}$ edge XMCD spectra. Inset (bottom panel): hysteresis curve of the peak A (associated to the Ni NPs phase) at 10 K for the higher fluence (Ni: 2×10^{17} ions cm^{-2}) sample.

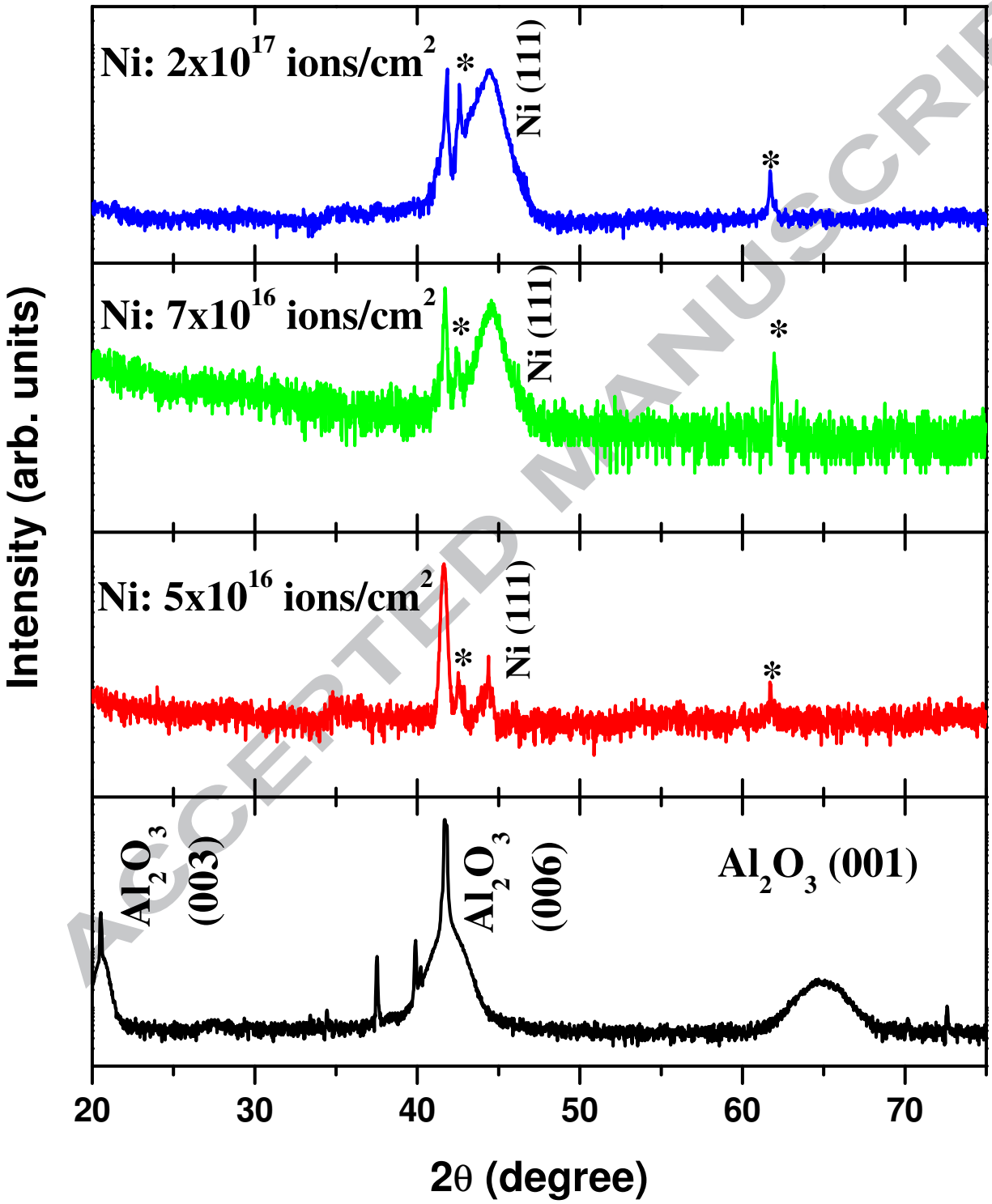

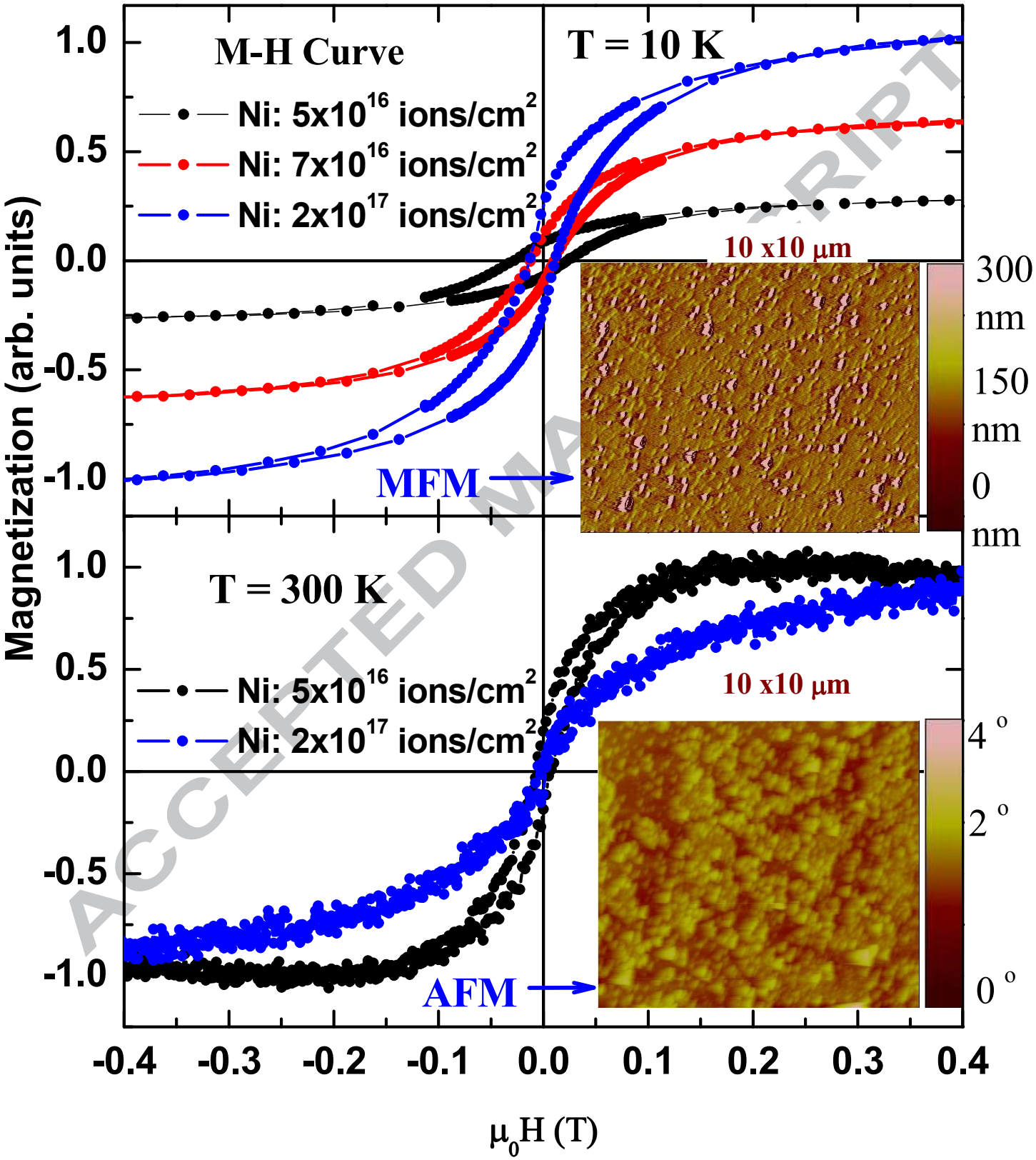

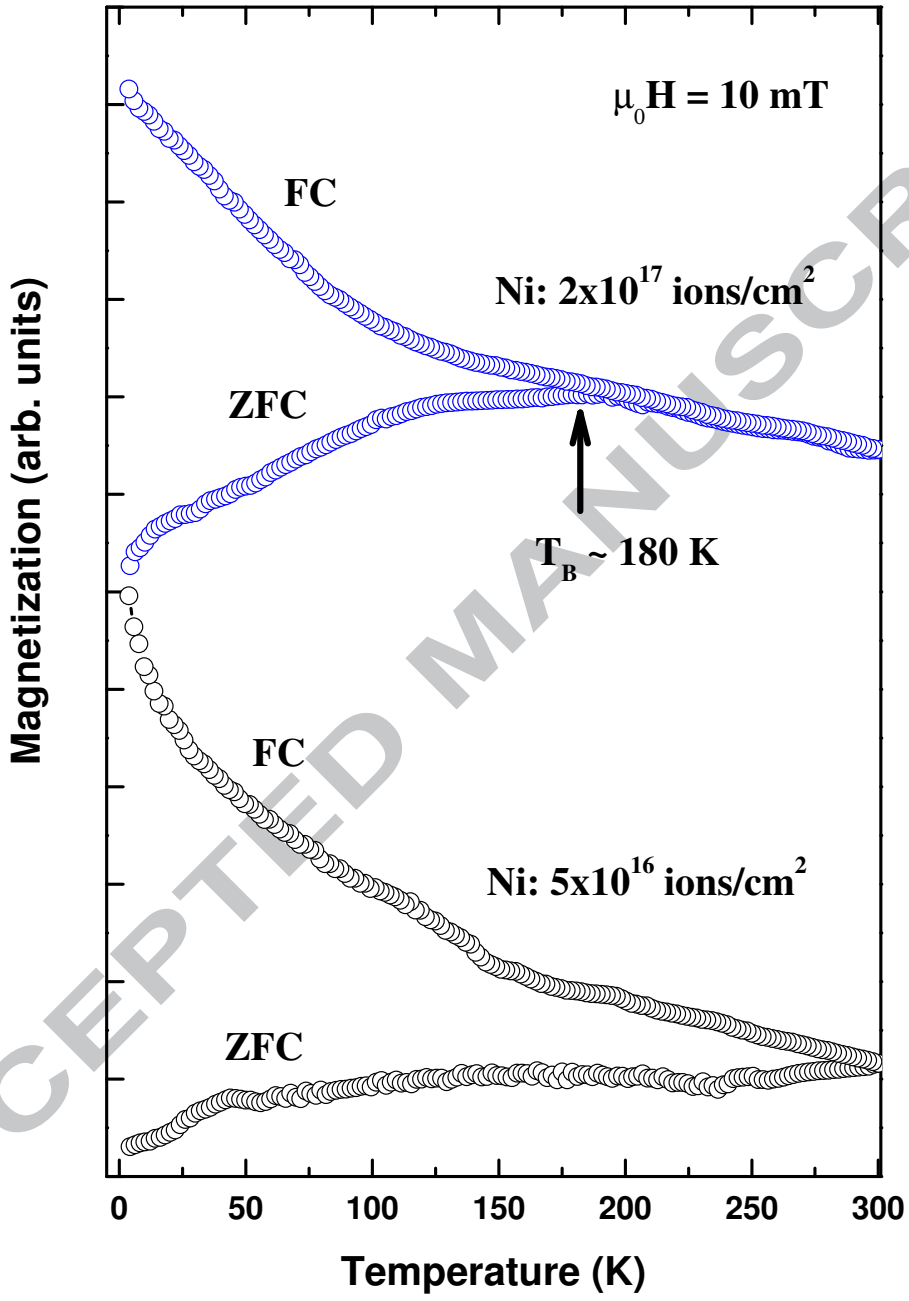

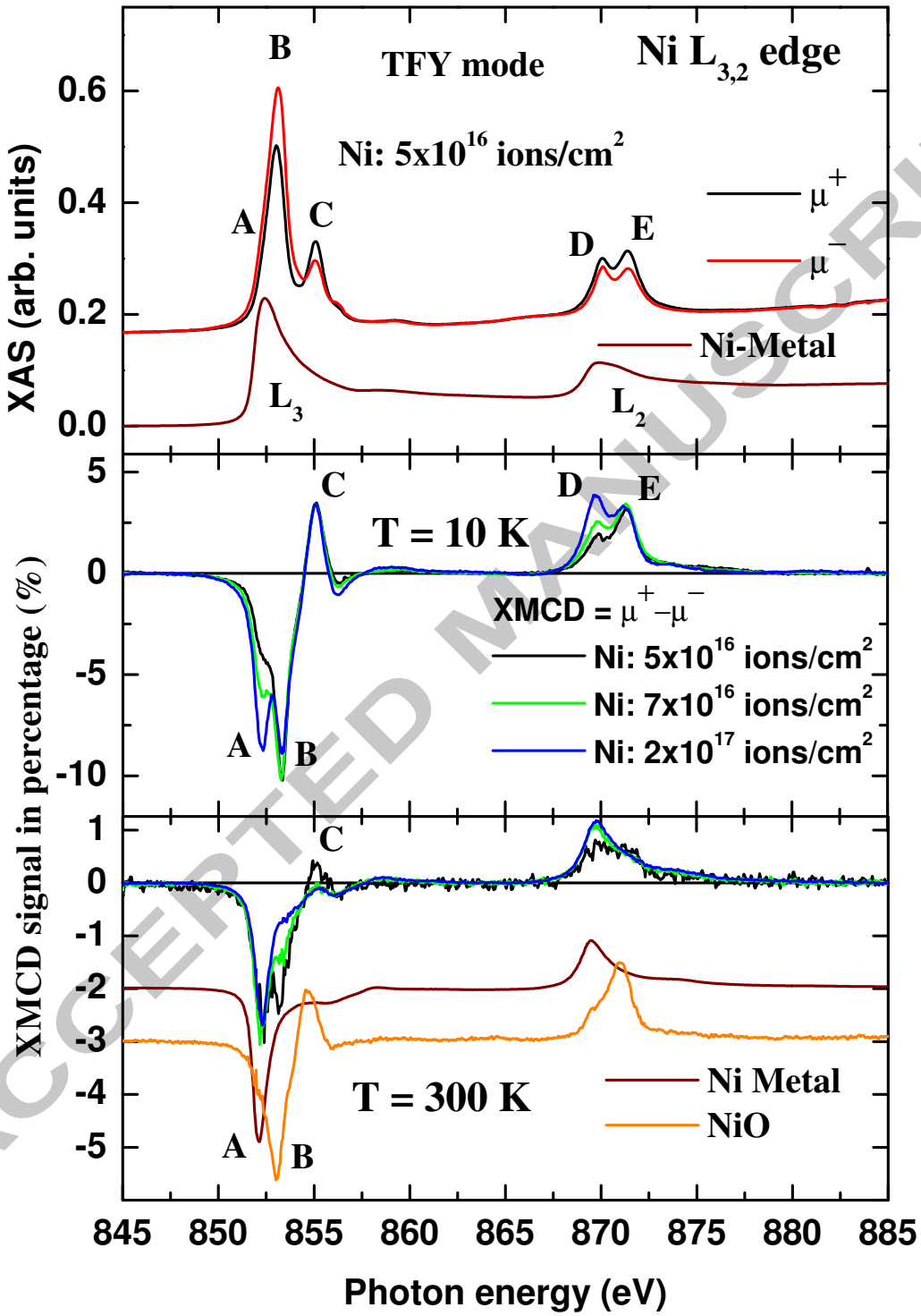

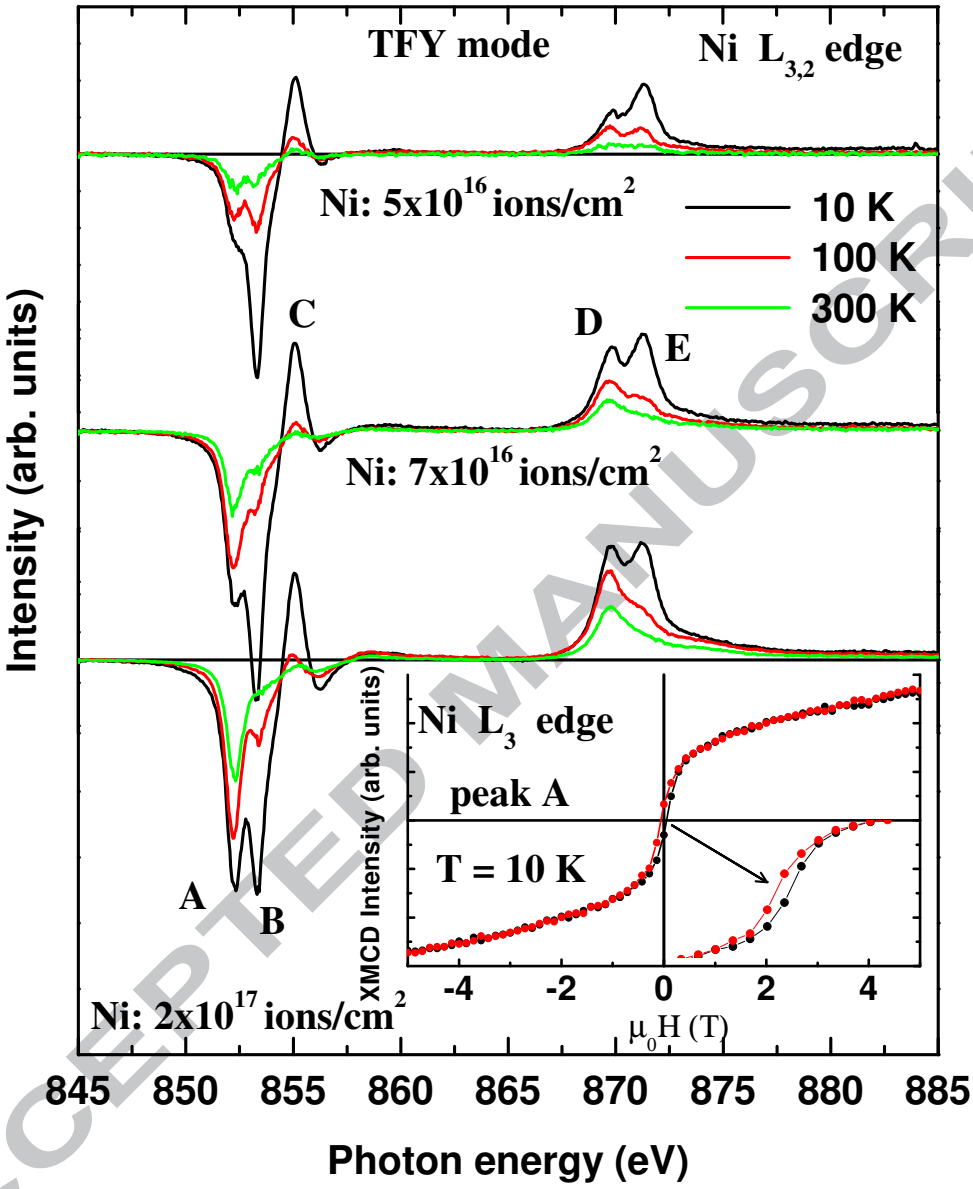

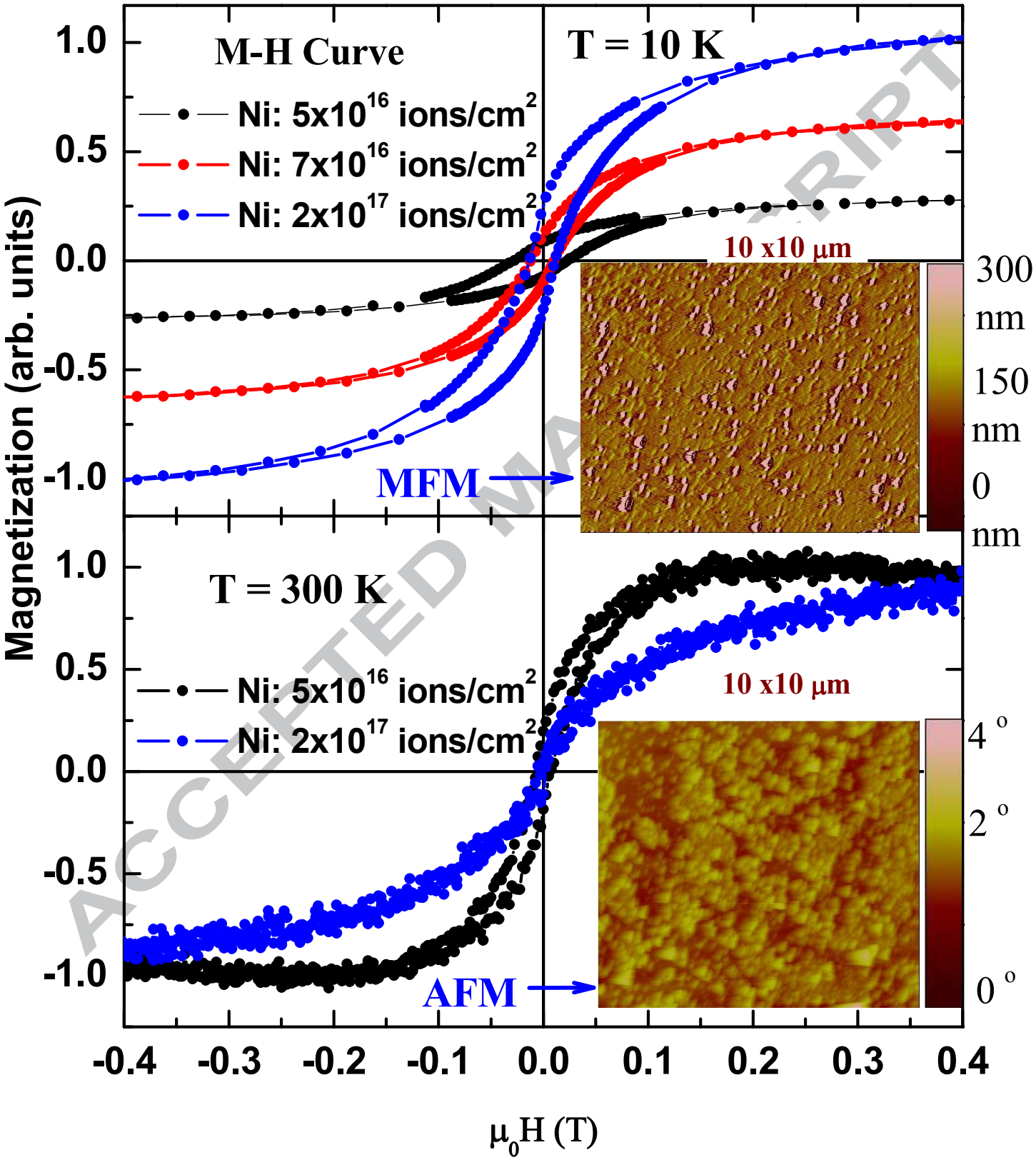

►A unique XAS/XMCD experiment of embedded nanoparticles in insulating/dielectric oxide matrix to distinguish magnetic contributions of different phases.

►Element-specific magnetic characterizations of Ni nanoparticles dispersed in sapphire (Al_2O_3-001) matrix prepared by ion-implantation (Ni:5×10^{16}-2×10^{17} ions cm^{-2}) has been investigated.

►We study the systematic evolutions of magnetic phases of Ni nanoparticles as a function of different Ni fluences and their magnetic response in the presence of other NiO_x phases.

►Our XMCD data provide a distinct "fingerprint" for the complex magnetic interactions between the nanophases of Ni NPs and NiO_x.